Preprint Volume, Symposium on the 50th. Anniversary of Operational Numerical Weather Prediction, American Meteorological Society, University of Maryland, College Park, MD, 23pp, 14-17 June, 2004.

P2.6 NOGAPS-ALPHA: A PROTOTYPE HIGH-ALTITUDE GLOBAL NWP MODEL

Stephen D. Eckermann, John P. McCormack, Lawrence Coy
Middle Atmosphere Dynamics Section, Naval Research Laboratory, Washington, DC

Douglas Allen
Middle Atmosphere Physics Section, Naval Research Laboratory, Washington, DC

Tim Hogan, Young-Joon Kim
Global Modeling Section, Naval Research Laboratory, Monterey, CA

1. INTRODUCTION

The Navy Operational Global Atmospheric Prediction System (NOGAPS) is the Department of Defense's (DoD's) high-resolution global numerical weather prediction (NWP) system. Its development and operation is a joint activity of the Naval Research Laboratory (NRL) and the Navy's Fleet Numerical Meteorology and Oceanography Center (FNMOC). NOGAPS is a complete operational forecasting system that includes data quality control (Baker 1992), tropical cyclone bogusing (Goerrs and Jeffries 1994), operational data assimilation (Daley and Barker 2001), balanced initialization (Errico et al. 1988), and a global forecast model (Hogan and Rosmond 1991; Hogan et al. 1991). Operational NOGAPS forecasts currently consist of high-resolution T239L30 six-day forecasts every 6 hours and once-a-day extended ten-day guidance using the FNMOC ensemble (T119L24). These forecasts are distributed to numerous defense and civilian users, and are used as input for numerous DoD environmental and application systems. Examples include: the Navy's Coupled Ocean-Atmosphere Mesoscale Prediction System (COAMPS™); FNMOC's ocean wave, sea ice, ocean thermodynamics, and tropical cyclone models; aircraft and ship-routing programs.

NOGAPS currently generates forecast fields from the ground to ~30 km. In October, 2000, NRL initiated an applied research project among its Space Science, Marine Meteorology and Remote Sensing Divisions to extend the vertical range of NOGAPS forecasts, initially to ~60 km, then progressively to ~80 km and then to ~100 km. This project is ongoing and has led to a new prototype NOGAPS global model with Advanced Level Physics and High Altitude (NOGAPS-ALPHA).

Developing NOGAPS-ALPHA involved significant changes in model configuration and implementation of new algorithms and physics/chemistry packages for the stratosphere and lower mesosphere. This paper summarizes this work, and also briefly illustrates some of the new capabilities that result (e.g., prognostic ozone). Other papers, both in this volume (Allen et al. 2004) and elsewhere (McCormack et al. 2004), will focus more specifically on the performance of

* Corresponding author address: Stephen D. Eckermann, E. O. Hulburt Center for Space Research, Code 7646, Naval Research Laboratory, Washington, DC 20375; e-mail: stephen.eckermann@nrl.navy.mil

NOGAPS-ALPHA as a global forecasting and modeling tool for the stratosphere.

2. THE NOGAPS GLOBAL SPECTRAL FORECAST MODEL (GSFM)

Hogan and Rosmond (1991) and Hogan et al. (1991) provide thorough descriptions of the NOGAPS forecast model. Briefly, NOGAPS is a global spectral model (GSM) in the horizontal and utilizes a generalized vertical coordinate within an energy conserving vertical finite difference formulation (Kasahara 1974; Simmons and Burridge 1981; Hogan and Rosmond 1991). The model's dynamical variables are relative vorticity, divergence, virtual potential temperature, specific humidity, and terrain (surface) pressure. The model is central in time with a semi-implicit treatment of gravity wave propagation and Robert (Asselin) time filtering (Simmons et al. 1978). The current operational model's physics packages include a bulk-Richardson number dependent vertical mixing scheme (Louis et al. 1982), a time-implicit Louis surface flux parameterization (Louis 1979), orographic gravity wave drag (Webster et al. 2003), shallow cumulus mixing of moisture, temperature, and winds (Tiedtke 1984), the Emanuel cumulus parameterization (Emanuel and Zivkovic-Rothman 1999; Peng et al. 2004), convective, stratiform and boundary layer cloud parameterizations (Slingo 1987; Teixeira and Hogan 2002), and a shortwave and longwave radiation scheme (Harshvardhan et al. 1987).

3. NOGAPS-ALPHA Developments

Our current prototype NOGAPS-ALPHA model extends to ~85 km in altitude, resolving the entire stratosphere and parts of the mesosphere. To accurately model these new upper-level regions of the atmosphere required developing, implementing and testing of a whole new family of algorithms and physics packages for the stratosphere and lower mesosphere.

Throughout this development process, particular attention has been paid to maintaining close connections between the NOGAPS-ALPHA GSM and the continually evolving operational NOGAPS. Whenever new tropospheric physics packages have been added to NOGAPS (e.g., Hogan et al. 2003; Peng et al. 2004), these new packages have also been quickly transitioned into NOGAPS-ALPHA. Additionally, any new physics package added to NOGAPS-ALPHA that purports to improve on an existing operational scheme never results in removal of the current operational scheme from the NOGAPS-ALPHA code. Instead, NOGAPS-ALPHA makes extensive use of "switches" which enable all the current operational and new ALPHA physics packages and algorithms to be activated or deactivated in various ways for any given run. This ensures that NOGAPS-ALPHA remains a high-altitude prototype of the current state-of-the-art NOGAPS GSFM running operationally at FNMOC.

We now summarize some of the more important new features in NOGAPS-ALPHA.

3a. Hybrid σ–p Vertical Coordinate

The NOGAPS GSM utilizes a vertical coordinate of the general Simmons and Strüfing (1983) analytical form

$$p(\eta_{k+1/2}, p_S) = A(\eta_{k+1/2}) + B(\eta_{k+1/2})[p_S - p_{TOP}]. \quad (1a)$$

Since the normalized model coordinate $\eta_{k+1/2}$ need not be defined explicitly in (1a) for use in the GSM, we reexpress (1a) using the implicit subscript notation

$$p_{k+1/2} = A_{k+1/2} + B_{k+1/2}[p_S - p_{TOP}], \quad (1b)$$

where $k=1,..,L$ is the integer full model layer number (from top to surface), $p_{k+1/2}$ are the $L+1$ half level interface pressures, p_S is the surface (terrain) pressure and p_{TOP} is the (constant) model top pressure. Through

judicious choices for the coefficients $A_{k+1/2}$ and $B_{k+1/2}$ at each hybrid level, (1) permits hybrid vertical model levels that transition from terrain-following (σ-like) levels near the ground to pure pressure levels in the stratosphere, subject to the boundary conditions $p_{1/2}=p_{TOP}$ ($A_{1/2}=p_{TOP}$, $B_{1/2}=0$, $\eta_{1/2}=0$) and $p_{L+1/2}=p_S$ ($A_{L+1/2}=p_{TOP}$, $B_{L+1/2}=1$, $\eta_{L+1/2}=1$).

NOGAPS has always used a coordinate defined in (1b) by setting $A_{k+1/2}=p_{TOP}$ at all levels k, so that $B_{k+1/2}=[p-p_{TOP}]/[p_S-p_{TOP}]$, (Hogan and Rosmond 1991), yielding a coordinate almost identical to the standard σ coordinate p/p_S (since $p_S \gg p_{TOP}$). Those levels for the current operational L30 model are plotted in Figure 1a.

In NOGAPS-ALPHA we now utilize the full functionality of (1b) by choosing $A_{k+1/2}$ and $B_{k+1/2}$ coefficients that give hybrid σ-p levels that transition smoothly from terrain following to isobaric in the stratosphere: Fels et al. (1980), Simmons and Burridge (1981) and Trenberth and Stepaniak (2002) provide motivation for using isobaric model levels in the stratosphere and mesosphere.

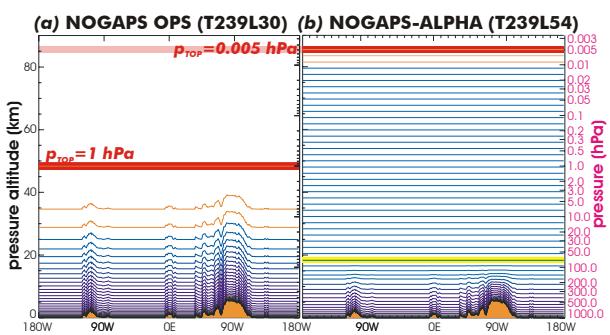

Figure 1: Vertical levels around a latitude circle at 34.5°N for: (a) operational NOGAPS T239L30 model, with p_{TOP}=1 hPa (red) and σ coordinate; (b) NOGAPS-ALPHA T239L54 model with p_{TOP}=0.005 hPa using our new hybrid σ–p formulation based on (1b) which transitions smoothly from terrain following to a first purely isobaric level at p_{INT}=72.6 hPa (k=34), shown in yellow. The top 2 full model layers in NOGAPS experience enhanced damping and diffusion to act as a sponge layer, and the top 3 model half levels bounding these top 2 layers are marked in orange.

Initially we implemented and tested a Sangster-Arakawa-Lamb (SAL) coordinate (Sangster 1960; Arakawa and Lamb 1977), which gives σ-like levels up to some interface pressure p_{INT} (typically ~70-100 hPa) and then isobaric levels from p_{INT} to p_{TOP}. The SAL hybrid coordinate is used in a number of global models: e.g., GFDL SKYHI (Fels et al. 1980), ARPEGE (Cariolle and Déqué 1986), and CAM2 (Collins et al. 2003).

However, the SAL coordinate has the disadvantage of producing sharp discontinuities in pressure height thicknesses at the pressure interface p_{INT} over high terrain, an effect that can yield large numerical errors in computed vertical gradient terms that are used in the governing equations (e.g., Simmons and Burridge 1981).

Consequently, for NOGAPS-ALPHA we have developed a more elaborate hybrid coordinate formulation that generates $A_{k+1/2}$ and $B_{k+1/2}$ coefficients that transition smoothly to isobaric levels without any abrupt discontinuities in layer thicknesses over mountains (achieved by ensuring that $(dB/d\eta)\rightarrow 0$ smoothly as $p\rightarrow p_{INT}$). The exact equations and procedures used, though straightforward, are lengthy and will be reported in full elsewhere. The hybrid model levels it produces for our standard L54 NOGAPS-ALPHA configuration with p_{TOP}=0.005 hPa are plotted in Figure 1b, illustrating the smooth transition to constant layer thicknesses in the stratosphere regardless of topographic elevation.

Operational NOGAPS uses model layer thicknesses that dilate rapidly with increasing model height through the stratosphere (Figure 1a). By contrast, our working NOGAPS-ALPHA formulation utilizes model layers with constant pressure height thicknesses of ~2 km throughout the stratosphere and lower mesosphere. From Figure 1, we see that undamped model layers in NOGAPS-ALPHA

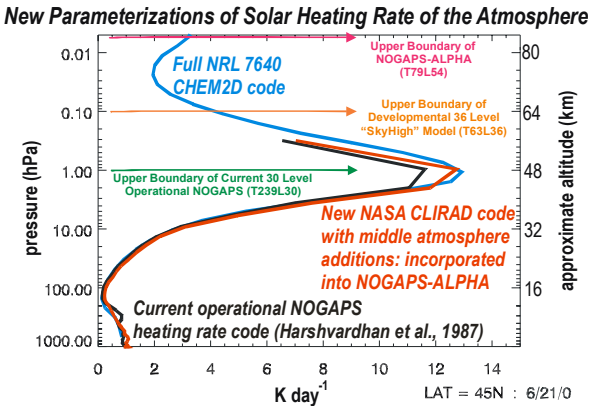

Figure 2: Profiles of diurnally-averaged shortwave heating (SW) at 45°N on 21 June using: (a) a detailed middle atmosphere SW radiation calculation from NRL's two-dimensional CHEM2D model (blue curve), which we use as validation for two NOGAPS-ALPHA schemes; (b) current NOGAPS scheme due to Harshvardhan et al. (1987) (black curve); (c) CLIRAD SW scheme due to Chou and Suarez (2002) (red curve). Note the differences in the upper stratosphere.

extend the vertical forecast range of the current operational model by a factor of ~3.

3b. CLIRAD Radiation Scheme

To provide more realistic radiative driving of the atmosphere, we have implemented the NASA "CLIRAD" longwave (LW) and shortwave (SW) schemes of Chou et al. (2001) and Chou and Suarez (2002), respectively. CLIRAD provides improved radiation calculations at all model levels, but significantly improves the middle atmosphere. For example, CLIRAD SW heating rates include contributions from O_2 and near-infrared CO_2 bands that are not contained in the current operational radiation scheme (Harshvardhan et al., 1987), which lead to underestimates in peak SW heating in the middle atmosphere of as much as 1-2 K day^{-1}, as shown in Figure 2.

To specify the global SW heating and LW cooling rate contributions from ozone (O_3) and water vapor (H_2O), NOGAPS utilizes seasonally-varying zonal-mean pressure-latitude lookup tables of their climatological mixing ratios, continually interpolating these values to the current forecast time and onto the NOGAPS model levels and Gaussian grid. For NOGAPS-ALPHA, the existing NOGAPS O_3 climatology of McPeters et al. (1984) was updated and extended vertically using the monthly mean O_3 climatology of Fortuin and Kelder (1998) (1000-0.3 hPa), while upper-level water vapor was prescribed using measurements (100-0.3 hPa) from the Halogen Occultation Experiment (HALOE) (Randel et al. 2001). At heights from 0.3 hPa up to 0.005 hPa, both O_3 and H_2O mixing ratios are based on long-term climate output from NRL's zonally-averaged CHEM2D dynamics-radiation-chemistry global model, which spans the ~0-108 km height range and includes very detailed middle atmospheric chemistry and radiation packages (Summers et al. 1997; McCormack and Siskind 2002).

Our goal is to ultimately replace these 2D climatological mixing ratios in the radiation calculations with three-dimensional (3D) NOGAPS-ALPHA prognostic chemical constituent fields, which are introduced and discussed in section 4. In NOGAPS-ALPHA we can already choose to use our developmental 3D prognostic ozone fields instead of 2D climatology within the CLIRAD radiation scheme to specify the O_3 LW and SW contributions.

3c. Upper Level Meteorological Initialization

In 2003, FNMOC replaced its Multivariate Optimal Interpolation (MVOI) data assimilation system (Goerrs and Phoebus 1992) with the new NRL Atmospheric Variational Data Assimilation System (NAVDAS), which is based on three-dimensional variational (3DVAR) analysis (Daley and Barker 2001). MVOI fields extended only to 10 hPa, though an experimental "STRATOI" product was also

issued, based mostly on TIROS-N Operational Vertical Sounder (TOVS) radiances, which yielded additional initialization wind, temperature and geopotential fields up to 0.4 hPa. Our test runs with NOGAPS-ALPHA to date have used MVOI/STRATOI fields almost exclusively. Newer NAVDAS fields currently extend to ~4 hPa, but should later extend to ~0.1 hPa when direct radiance assimilation comes online. Thus, to initialize NOGAPS-ALPHA we must for now supplement current operational meteorological initialization fields with some working representation of the atmospheric state between p_{TOP}=0.005 hPa and the top operational analysis level p_{AN}.

Our current approach is to extrapolate the topmost analysis temperatures and zonal and meridional wind fields upwards and then progressively relax the extrapolated profiles with increasing altitude towards monthly varying zonal-mean climatological values. For temperature, the equations used are

$$T(\lambda,\varphi,p)=\left[1-w(p)\right]T_{LE}(\lambda,\varphi,p)+w(p)T_{CLIM}(\varphi,p) \tag{2a}$$

$$w(p)=\left\{\frac{\ln p_{AN}-\ln p}{\ln p_{AN}-\ln p_{TOP}}\right\}^{\varepsilon}, \tag{2b}$$

where λ is longitude and φ is latitude. $T_{CLIM}(\varphi,p)$ are zonal-mean climatological temperatures. $T_{LE}(\lambda,\varphi,p)$ are "lapse-rate extrapolated" temperatures in which the analysis temperatures at the top analysis level, $T(\lambda,\varphi,p_{AN})$, are extrapolated upwards using the climatological lapse rates dT_{CLIM}/dp. Figure 3a shows how the final profile $T(\lambda,\varphi,p)$ at altitudes above p_{AN} is formed as the weighted sum of these two profiles, as specified in (2).

The normalized weighting coefficient $w(p)$ in (2b) increases monotonically with increasing log-pressure altitude, such that $w(p_{AN})$=0 and $w(p_{TOP})$=1, so that the fit (2a) contains pure analysis at p_{AN}, mostly extrapolated analysis near p_{AN} (to retain close connections with analyzed fields), but relaxes to pure climatology at p_{TOP}. The rate at which $T(\lambda,\varphi,p)$ reverts to climatology is controlled by the coefficient ε in (2b). For small (large) ε, (2a) transitions more rapidly (gradually) with altitude to climatology. Currently we use ε=1 in NOGAPS-ALPHA. The climatological fields we use are monthly zonal-mean zonal winds, temperatures and geopotential heights from the 1986 COSPAR International Reference Atmosphere (CIRA) (Fleming et al. 1990), interpolated to the initialization time and model pressures and latitudes. The final temperature profile (2a) in turn yields a geopotential profile though the hydrostatic relation

$$\phi(\lambda,\varphi,p)=\phi_{AN}+R\int_{p_{AN}}^{p_{TOP}}T(\lambda,\varphi,p)d\ln p \tag{3}$$

where $\phi_{AN}=\phi(\lambda,\varphi,p_{AN})$ and R is the gas constant.

Winds are dealt with slightly differently to temperatures. As shown in Figure 3b, we perform a direct upward extrapolation of

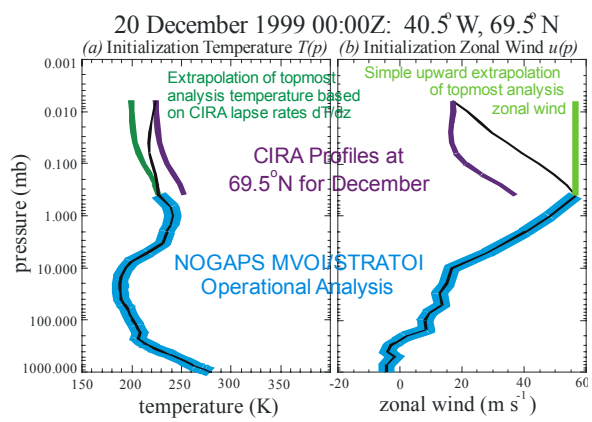

Figure 3: Black curve shows NOGAPS-ALPHA initialization of (a) temperature and (b) zonal winds for 20 December 1999 0:00Z at a sample location of 40.5°W, 69.5°N. Other curves show: NOGAPS MVOI/STRATOI operational analysis (aqua curve); profiles extrapolated upwards from top analysis level using CIRA lapse rates (dark green) and constant wind (light green). Purple curves show CIRA climatology for December at 69.5°N. Final profile is a progressively weighted fit between the green and purple curves, yielding pure analysis (green) at 0.4 hPa and pure CIRA climatology (purple) at p_{TOP}=0.005 hPa.

winds at the top analysis levels and progressively blend these with climatological winds using (2b). Given the unreliability of mesospheric CIRA zonal winds during certain months, particularly near the equator (Randel et al. 2004), we have added an additional option of relaxing zonal winds to either CIRA or the more recent climatological zonal wind fields from the UARS Reference Atmosphere Project (URAP) (Swinbank and Ortland 2003). Since we have no reliable meridional wind climatology at upper altitudes, we currently relax meridional winds to a reference climatology field set to zero everywhere, yielding vanishing meridional winds initially at p_{TOP}.

In addition to our standard operational NAVDAS fields, we have developed strategies for ingesting into NOGAPS-ALPHA initialization fields from other NWP centers, such as the European Centre for Medium-Range Weather Forecasts (ECMWF) and the National Centers for Environmental Prediction (NCEP): see Allen et al. (2004) for more details.

3d. Gravity Wave Drag

The importance of parameterized subgrid-scale orographic gravity wave drag (GWD) for improved forecast skill in the troposphere is well known (e.g. Kim et al. 2003; Webster et al. 2003). On extending the vertical range of NWP models into the stratosphere and mesosphere, GWD parameterization becomes an even more important and general issue, since the circulations of the entire equatorial stratosphere and global mesosphere are driven by large synoptic-scale body forces maintained by quasi-continuous gravity wave breaking around the globe (Fritts and Alexander 2003). Even high-resolution global NWP models like NOGAPS cannot adequately resolve this GWD (Kim et al. 2003).

For NOGAPS-ALPHA we have developed and implemented a number of new GWD schemes. We have implemented three separate orographic GWD schemes, any one of which can be activated for a given run. Two are operational schemes: the Palmer et al. scheme (Palmer et al., 1986), which was used operationally in NOGAPS for many years, and the newer scheme of Webster et al. (2003), which replaced it in 2003 (Hogan et al., 2003). The third scheme is a more complex developmental scheme of Kim and Doyle (2004) that extends earlier work of Kim and Arakawa (1995), a version of which is implemented currently in the NCEP GSM (Alpert et al. 1996). Kim and Hogan (2004) report on momentum budget studies with NOGAPS using this scheme. A parameterization of GWD due to convectively generated waves has also been developed and installed (Chun and Baik 2002).

In the stratosphere and mesosphere, gravity wave amplitudes become large and there is greater interaction among a larger number of waves, leading to less obvious signatures of individual wave packets from identifiable tropospheric sources like mountains and deep convection (Fritts and Alexander, 2003). Thus, we have also implemented and begun testing several spectral GWD schemes that have become popular recently for parameterizing GWD from a broad spectrum of waves in the middle stratosphere and above. We have implemented the Alexander and Dunkerton (1999) scheme into NOGAPS-ALPHA, generalizing it to multiple wave propagation azimuths. We have tested it in a series of 12-24 month runs in efforts to tune it to generate a realistic semiannual zonal wind oscillation (SAO) in the tropical stratosphere and lower mesosphere.

We have also investigated coupling among various schemes that might provide a more integrated GWD product for NOGAPS-ALPHA. We have coded the so-called

"Doppler-spread" spectral GWD scheme of Hines (in collaboration with B. N. Lawrence from Rutherford-Appleton Laboratory) and can couple it with our orographic GWD schemes, in the general manner outlined by Hines (1997). We have also investigated ways in which our orographic and convective GWD schemes lower down might be coupled to an Alexander-Dunkerton spectral scheme higher up. However, given the complexity of these developmental coupled schemes, we are currently testing them offline in single-column tests using NOGAPS-ALPHA model grids and fields.

Figure 4 shows an example of single column NOGAPS-ALPHA tests of some of these individual (uncoupled) GWD schemes. This case uses model fields at +114 hours from a NOGAPS-ALPHA T79L54 forecast run initialized from MVOI/STRATOI fields on 17 January 2003 at 0:00Z. Figures 4a and 4b show zonal wind and temperature, respectively, over southern Scandinavia. At this time (21 Feburary, 18:00Z) a dynamical stratospheric warming event was well underway and the vortex temporarily split (e.g., deZafra and Muscari 2004; McCormack et al. 2004). The warming is evident from the enhanced NOGAPS-ALPHA stratopause temperature compared to CIRA climatology.

The middle row of plots shows mean-flow accelerations (MFAs) due to parameterized orographic drag from flow across the southern Kjønas Mountains, as specified by the Palmer et al. GWD scheme (Figure 4c) and the Webster et al. scheme (Figure 4d). The differences are broadly consistent with some large differences in physics between these two schemes: the newer Webster et al. scheme produces much larger flow blocking drag near the surface and transfers a much smaller fraction of the total surface pressure drag across the mountains into propagating mountain waves, compared to the Palmer et al. scheme (Webster et al., 2003). This explains the significant surface MFA and much smaller

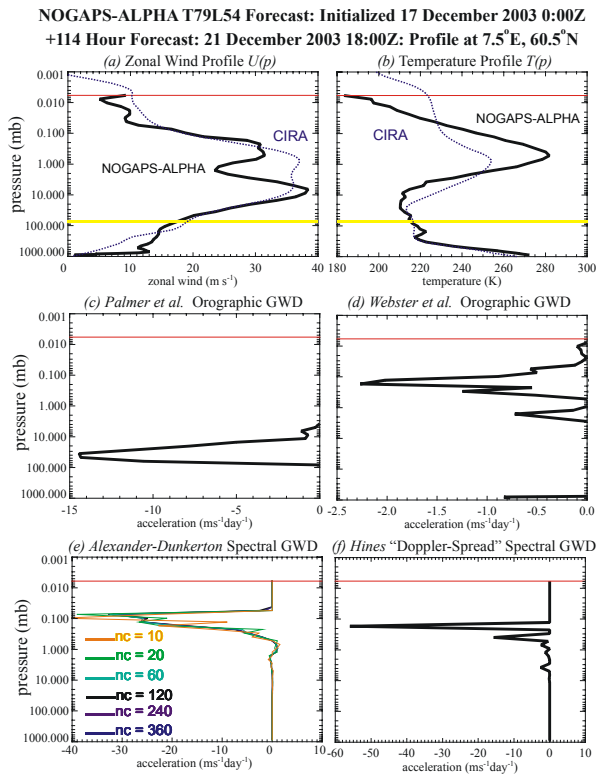

Figure 4: (a) Zonal wind and (b) temperature over southern Scandinavia (7.5°E, 60.5°N) from a NOGAPS-ALPHA T79L54 +114 hour forecast initialized on 17 January 2003 at 0:00Z. Middle row shows zonal mean-flow accelerations from orographic GWD from (c) Palmer et al. and (d) Webster et al. schemes. Bottom row shows mean-flow accelerations from spectral GWD schemes of (e) Alexander-Dunkerton (AD) and (f) Hines. The AD profiles show sensitivity of profile to number of phase speeds *nc* in the spectrum. Red curve shows p_{TOP} and yellow curve shows p_{INT}.

stratospheric MFAs in Figure 4d compared to the Palmer et al. profile in Figure 4c.

Figure 4e shows a series of MFA profiles computed using the spectral scheme of Alexander and Dunkerton (1999), illustrating one of numerous tuning experiments needed when implementing such schemes. These profiles investigate the sensitivity of the MFA profile to one particular parameter: the number of individual phase speeds *nc* in the wave spectrum. We see the profiles generally overlay for $nc \gtrsim 120$. This wave spectrum was launched at 15 km, with a phase speed width

c_w=60 m s^{-1} centered about the local mean wind at 15 km, peak momentum flux per unit mass B_m=0.4 m^{2}s^{-2}, a horizontal wavelength of 100 km, and total flux per unit mass F_{S0}=0.0004m^{2}s^{-2}. This spectrum is launched at 3 different propagation azimuth pairs: 0/180°, 45/225°, and -45/135°. All these parameters must be tuned carefully too for acceptable middle atmospheric circulations (e.g., Alexander and Rosenlof, 2003).

Figure 4f illustrates a similar run with the Hines (1997) spectral scheme. The MFA profile is generally similar though less smooth vertically, consistent with findings in some previous studies which show that the Hines scheme deposits wave fluxes more abruptly at high altitudes rather than smoothly over a more extended altitude range (Charron et al. 2002).

As with lower atmospheric schemes, these upper atmospheric GWD schemes need to be carefully tuned to yield acceptable circulations (e.g., Figure 4e), which, given their complexity, is a time-consuming process and necessitates retuning whenever horizontal or vertical model resolution is changed. Rayleigh friction (RF) can also be used: while RF is a much cruder proxy for mesospheric GWD and can have deleterious side effects, such as suppression of local dynamical variability and the potential for unrealistic secondary circulations (Shepherd et al. 1996), it has the advantage of being more easily tunable and so is used in the upper boundaries of many global NWP models (e.g., Butchart and Austin 1998). Thus we have also implemented a general RF scheme for simpler middle-atmospheric GWD specification, which currently allows the user to choose from any one of nine prescribed RF profiles. As shown in Figure 5, these profiles range from weak to strong and (vertically) shallow to deep drag, and are all based on profiles used in other global middle-atmosphere model studies (Boville 1986; Shepherd et al. 1996; Butchart and Austin 1998; Pawson et al. 1998; Limpasuvan et al. 2000).

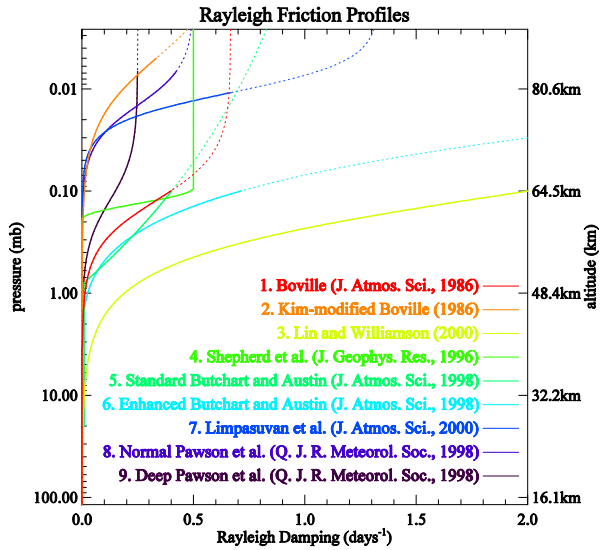

Figure 5: Various Rayleigh friction profiles (expressed as damping rates) available for use in NOGAPS-ALPHA, based on profiles used in some other global models and spanning various ranges of required damping. Each profile was chosen for a specific model with a differing p_{TOP}, and those tops for each model are marked by a change from solid to dotted curves in each case.

4. FULL PROGNOSTIC CAPABILITY FOR TRACE CHEMICAL CONSTITUENTS

Another major addition to NOGAPS-ALPHA has been full 3D prognostic capabilities for key trace chemical constituents, such as ozone. Just as for meteorological variables, full prognostic chemistry capability requires many features, including 3D global initialization, accurate global advection (adiabatic tendencies) and, where necessary, photochemical and/or microphysical updating (diabatic tendencies). We devote a separate section here to describing this new capability.

4a. Initialization

The number of specific chemicals to be used in any given NOGAPS-ALPHA run is

specified by various logical switches at run time. NOGAPS-ALPHA currently supports initialization (and subsequent forecasting) of the following minor constituents: water vapor (H_2O), ozone (O_3), nitrous oxide (N_2O), and methane (CH_4). In addition, each chemical can be forwarded in either a "passive" mode (no chemistry/microphysics, purely passive transport), or "active" mode (chemistry/microphysics activated), allowing for a total of 8 different types of prognostic chemical fields. The passive and active chemical pairs prove particularly valuable when assessing new parameterized chemistry schemes in NOGAPS-ALPHA, since subtracting the two fields allows us to factor out transport and thus isolate the accumulated chemistry effects within air parcels at specific locations.

However, active water vapor has always been an intrinsic model variable in NOGAPS, since it enters the GSM's governing equations of motion through the virtual potential temperature (Hogan and Rosmond 1991): thus, the model treats "active H_2O" as a meteorological field, reducing the total number of possible chemical fields to 7, including passive H_2O.

Water vapor is initialized as in NOGAPS, using 3D analyzed dew point depression fields, which are subsequently converted to specific humidity fields. These fields do not currently extend much above 10 hPa and so the 10 hPa analyzed humidity fields are simply extrapolated to upper altitudes in NOGAPS-ALPHA, which, given the relative dryness of the stratosphere and mesosphere, is an acceptable short-term solution.

Ozone can be initialized in one of two ways in NOGAPS-ALPHA. While NAVDAS does not at present assimilate O_3 operationally, there are plans to do and so we have developed code in NOGAPS-ALPHA to ingest and initialize such 3D initialization fields whenever they become available. In the meantime, to test and utilize this capability we have generated proxy three-dimensional analyzed O_3 mixing ratio fields for NOGAPS-ALPHA runs based on the O_3 analyses issued by both the NASA Global Modeling and Analysis Office (GMAO) (Stajner et al. 2001) and the ECMWF (Dethof 2003). When activated, NOGAPS-ALPHA searches for 3D ozone pressure-level initialization fields for the date in question, reads them in and then interpolates them onto model levels and the Gaussian grid. Since these analyzed ozone fields currently abate at p_{AN} ~ 0.2-1 hPa, for now we extrapolate O_3 mixing ratios at this top analysis level upwards to p_{TOP} in a manner similar to zonal wind, as shown in Figure 3b (green curve). In future we will develop a better extrapolation procedure that relaxes to the 2D climatology, in a manner somewhat similar to that for temperature fields, as illustrated in Figure 3a.

When 3D O_3 analysis fields are not available, we can instead initialize our 3D chemical field using the zonally averaged two-dimensional (2D) NOGAPS-ALPHA O_3 climatological fields described in section 3b.

For N_2O and CH_4, operational 3D analyses do not currently exist, and so our current strategy is to initialize these fields using 2D climatologies. Our 2D N_2O and CH_4 climatologies for NOGAPS-ALPHA were derived from multi-year simulations using CHEM2D (McCormack and Siskind 2002), and extend from 1000 to 0.001 hPa.

4b. Chemical Advection

Once initialized, these chemical fields are transported globally within the GSM using the same spectral advection algorithms used to advect meteorological variables such as vorticity and specific humidity. Over time, spectral advection yields fine scale spectral noise in the chemical fields (Rasch and Williamson 1990; Fairlie et al. 1994), which we effectively suppress through the use of a small amount of ∇^4 horizontal spectral

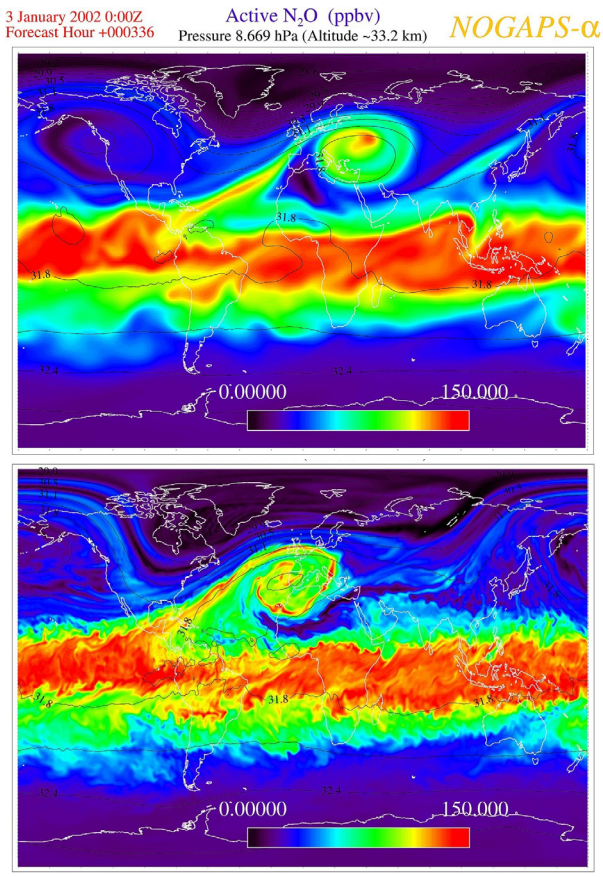

Figure 6: NOGAPS-ALPHA +336 hour forecasts of active N_2O at 8.7 hPa based a run initialized on 20 December 2001 at 0:00Z. Top plot shows T79L54 run, bottom plot shows T239L54 run. Values in color bar are mixing ratios in ppbv, contours are geopotential height in kilometers

diffusion after each time step. This can be applied either to the isobaric stratospheric levels only, or to all the hybrid model levels.

4c. Photochemistry

For direct simulations of stratospheric ozone photochemistry, a reasonable simulation would require at least 60 different chemical reactions involving ~40 different minor chemical species. At this early stage of our development, this is impractical and so we have pursued simpler parameterization strategies that yield acceptably accurate photochemical tendencies over forecast time scales.

We have focused to date on linearized ozone photochemistry schemes that parameterize the major production/loss rate dependences globally through climatological lookup tables, which are generated by a middle atmospheric climate model containing sophisticated radiation and chemistry packages. For NOGAPS-ALPHA, we use NRL's CHEM2D model for this purpose (Summers et al. 1997; McCormack and Siskind 2002).

Nitrous Oxide

We implemented prognostic N_2O in NOGAPS-ALPHA primarily because its photochemistry is relatively simple, and thus it is a good candidate chemical for developing an initial parameterized photochemistry scheme. However, prognostic N_2O is a useful quantity to implement for other reasons too: it has important radiative effects, destroys ozone (indirectly, via NO_x products from N_2O photodissociation), and has slow photochemical rates and sharp gradients both vertically and latitudinally that make it an excellent diagnostic pseudo-tracer of the atmospheric motion. Furthermore, in the stratosphere it is well measured by a number of satellite instruments (e.g., Urban et al. 2004) and thus its prognostic output from NOGAPS-ALPHA runs can be validated globally.

N_2O is produced at the surface by biological and anthropogenic activity (e.g., Huttunen et al. 2003; Scanlon and Kiely 2003) and is destroyed in the stratosphere primarily by photolysis (Brasseur and Solomon 1984). In parameterizing this loss, we follow the approach of Randel et al. (1994) and parameterize it using the rate equation

$$\frac{d\chi_{N_2O}}{dt} = -\frac{\chi_{N_2O}}{\tau_{N_2O}(\varphi, p, t)} \quad , \qquad (4)$$

where *d/dt* is the advective time derivative, $\chi_{N_2O}(\lambda, \varphi, p, t)$ are N_2O mixing ratios, and

$\tau_{N_2O}(\varphi, p, t)$ are the N_2O loss rates: the latter are derived from diurnally-averaged output from long-term CHEM2D runs, then output as lookup tables as a function of latitude, pressure and month. These loss rates are generally slow, peaking in the equatorial stratosphere at altitudes ~30-40 km. The tabulated loss rate values are continually interpolated within NOGAPS-ALPHA to the precise location and forecast time and date in question. We approximate source production by keeping the surface-level mixing ratios set to 320 ppbv.

Figure 6 shows prognostic N_2O fields after 14 days in two NOGAPS-ALPHA runs at T79L54 and T239L54, with otherwise identical initial conditions and model parameter settings. Both plots show a strong wave breaking event in which high-N_2O tropical air, typically isolated from mid-latitudes by a subtropical transport barrier (Neu et al. 2003), is rapidly pulled out to midlatitudes in a thin streamer that then wraps around into a vortex-like structure over western Europe. Close inspection of both plots shows considerable similarity, particularly in the Southern Hemisphere, illustrating the robust nature of these prognostic N_2O fields, and in particular the fidelity of the NOGAPS-ALPHA spectral code for chemistry advection. Slight differences are apparent: the streamer event in the T239L54 run is longitudinally displaced from a similar looking event in the T79L54 run, which is a meteorological effect possibly associated with greater explicitly resolved GWD in the T239L54 run that slightly modifies the mean-flow evolution between the two runs.

Methane

Our success in parameterizing N_2O photochemistry motivated us to develop a similar chemistry scheme for CH_4. Like N_2O, CH_4 is radiatively important, affects odd-oxygen photochemistry, and is measured

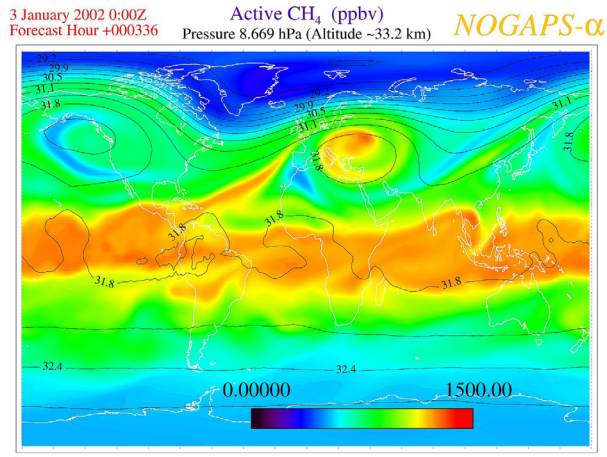

Figure 7: NOGAPS-ALPHA +336 hour forecasts of active CH_4 at 8.7 hPa based a T79L54 run initialized on 20 December 2001 at 0:00Z. Values in color bar are mixing ratios in ppbv, contours are geopotential height in kilometers.

globally from space. Additionally, methane oxidation is an important source of water vapor for the upper stratosphere: a simple one-dimensional methane oxidation parameterizaton was instituted in the ECMWF model to account for this high-altitude moisture source for their 3D prognostic water vapor fields. Thus, an ability to generate prognostic CH_4 in NOGAPS-ALPHA could then also allow this stratospheric moisture source to be parameterized three-dimensionally through conservation of the "potential hydrogen" term $2\chi_{CH_4} + \chi_{H_2O}$ (Summers et al. 1997).

Similar to N_2O, CH_4 is produced at the surface and is destroyed in the middle atmosphere primarily by reactions with OH, $O(^1D)$, chlorine and Lyman-α photolysis (Brasseur and Solomon 1984). We have parameterized CH_4 chemistry in NOGAPS-ALPHA using an equation identical to form to (4), with the $\tau_{CH_4}(\varphi, p, t)$ diurnally averaged loss rates again generated from CHEM2D runs. Figure 7 plots prognostic CH_4 mixing ratios after 14 days for a T79L54 NOGAPS-ALPHA run with the same meteorological initial conditions and very similar

parameterization settings to the N_2O T79L54 run depicted in Figure 6, and shows a similar streaming of high CH_4 tropical air to midlatitudes by a wave breaking event.

Ozone

Ozone photochemistry requires a considerably more complicated parameterization, since it is continuously created and destroyed in the middle atmosphere. In our initial implementations, we have pursued a linearized photochemistry approach, which begins by postulating a set of core model variables that have the greatest perceived impact on net ozone (odd-oxygen) production and loss rates, *(P-L)*. Extensive stratospheric ozone research has established that production/loss of ozone is most sensitive to the current local value of the ozone mixing ratio, χ_{O3}, the local temperature T, and the local intensity of UV radiation, which in turn depends on the overhead vertical column amount of ozone, c_{O3}, via the shielding effect. We express this functionally as

$$\frac{d\chi_{O_3}}{dt} = (P-L)\left[\chi_{O_3}, T, c_{O_3}\right] \quad . \tag{5}$$

We approximate the function on the right-hand side of (5) using a standard truncated (linearized) Taylor series expansion (McLinden et al. 2000)

$$(P-L) = (P-L)_0 + \left.\frac{\partial(P-L)}{d\chi_{O_3}}\right|_0 \left(\chi_{O_3} - \bar{\chi}_{O_3}\right) + \left.\frac{\partial(P-L)}{dT}\right|_0 \left(T - \bar{T}\right) + \left.\frac{\partial(P-L)}{dc_{O_3}}\right|_0 \left(c_{O_3} - \bar{c}_{O_3}\right). \tag{6}$$

The subscript "0" denotes values computed at some reference state $\bar{\chi}_{O_3}$, $\bar{T}$, and $\bar{c}_{O_3}$, which ideally should be a chemical equilibrium state but, when implemented as a parameterization in models, tends to work better using reference climatologies. Thus $(P-L)_0$ and its 3 partial derivative terms in (6) can all be evaluated with global models containing full radiation and chemistry (e.g., CHEM2D) via a series of simulations that evaluate net rates about this reference state and then perturb that state with respect to the mixing ratio, temperature, and column amount to estimate the partial derivative terms. The 4 linearized photochemical coefficients in (6) can then be progressively estimated and issued as latitude-pressure-month lookup tables.

Observational validation for this linearized approach (6) to parameterizing O_3 photochemistry exists. Linearized photochemistry has been used successfully to model observed ozone-temperature correlations in the stratosphere (e.g., Douglass et al. 1985; Stolarski and Douglass 1985) and various types of stratospheric planetary wave signals seen in satellite ozone data (e.g., Randel and Gille 1991; Randel 1993; Smith et al. 2002).

We have developed and implemented 3 separate O_3 photochemistry schemes for NOGAPS-ALPHA based on this particular parameterization approach, any one of which can be selected by the user for prognostic ozone runs.

CHEM2D scheme

As with our N_2O and CH_4 schemes, we have run CHEM2D to generate O_3 linearized photochemical coefficients. An important point to note is that, while our focus is on ozone, the linearized photochemical coefficients themselves relate most directly to the odd-oxygen (O_x) photochemistry (O_3 + O) that governs net O_3 production/loss, rather than the individual O_3 rates themselves. At an equilibrium O_x state, there is still constant rapid chemical cycling between ozone and monatomic oxygen, so that the lifetime of individual O_3 molecules is short yet total O_3 mixing ratios do not change (Brasseur and Solomon 1984). The CHEM2D runs needed to

generate these linearized O_3 photochemical coefficients are much more challenging and time-consuming than for N_2O and CH_4, and to date we have generated and validated only the first two linearized photochemistry terms in (6). We express these here as

$$\frac{d\chi_{O_3}}{dt} = (P-L)_0^{CHEM2D}[\varphi,p,t] - \frac{\left(\chi_{O_3} - \overline{\chi}_{O_3}\right)}{\tau_{O_3}^{CHEM2D}(\varphi,p,t)} \quad (7a)$$

where

$$\tau_{O_3}^{CHEM2D}(\varphi,p,t) = -\left[\left.\frac{\partial(P-L)}{d\chi_{O_3}}\right|_0\right]^{-1} \quad (7b)$$

is the ozone photochemical relaxation time scale, and for $\overline{\chi}_{O_3}$ we relax to the new 2D ozone climatology discussed in section 3b. The NOGAPS-ALPHA lookup tables for our CHEM2D ozone relaxation times are plotted for June and December in Figures 8a and 8b, respectively. The time scale is very long in the lower stratosphere where ozone is tracer-like, and short in the upper stratosphere where photochemistry is dominant. The rates also get very long at all heights in polar night where no sunlight is available to drive the photochemistry.

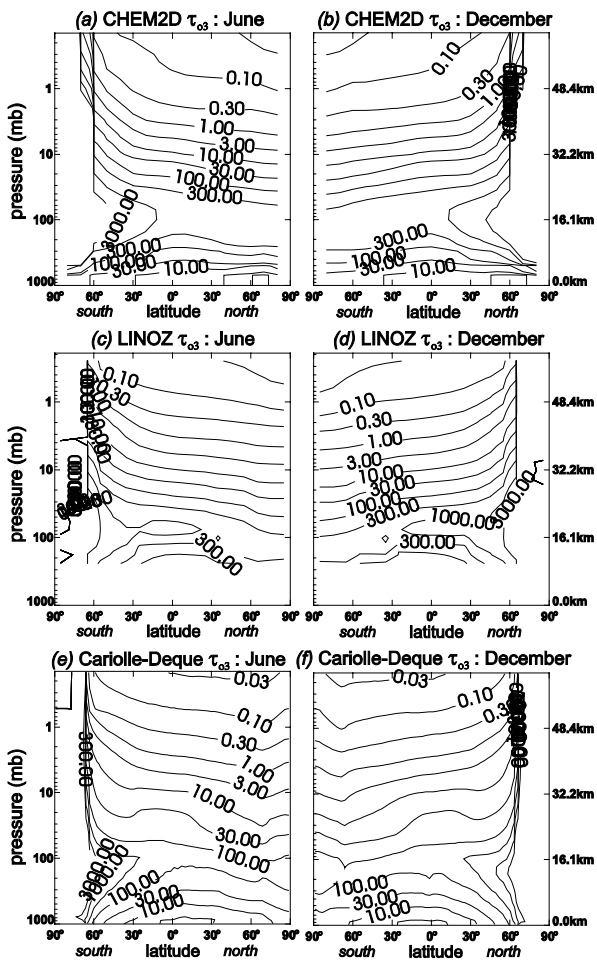

Figure 8: Ozone photochemical relaxation times, in days, for June and December for CHEM2D scheme (top row), LINOZ scheme (middle row) and Cariolle-Déqué scheme (bottom row).

LINOZ scheme

Two linearized ozone photochemistry schemes based on (5)-(6) already exist, for which we have obtained the 4 governing linearized photochemical coefficients. The first is the so-called LINOZ scheme of McLinden et al. (2000). The LINOZ coefficients were computed using the University of California, Irvine photochemistry box model. The scheme relaxes via (6) to reference 2D climatologies for ozone, temperature and ozone column abundances published in technical reports from NASA's Airborne Effects of Stratospheric Aircraft (AESA), which we also obtained. The LINOZ ozone photochemical time scales for June and December are plotted in Figures 8c and 8d, respectively, and span the 0.25-250 hPa range only: above and below these boundaries, we extrapolate the boundary values upwards and downwards respectively while zeroing out the other extrapolated photochemical coefficients, yielding a simple relaxation to the ozone climatology.

Cariolle-Déqué scheme

A full version of (5)-(6) was developed in the mid-eighties by Cariolle and Déqué (1986) using their two-dimensional chemistry model, for use in their 3D climate model. That same basic scheme has recently been incorporated into the ECMWF model, with linearized

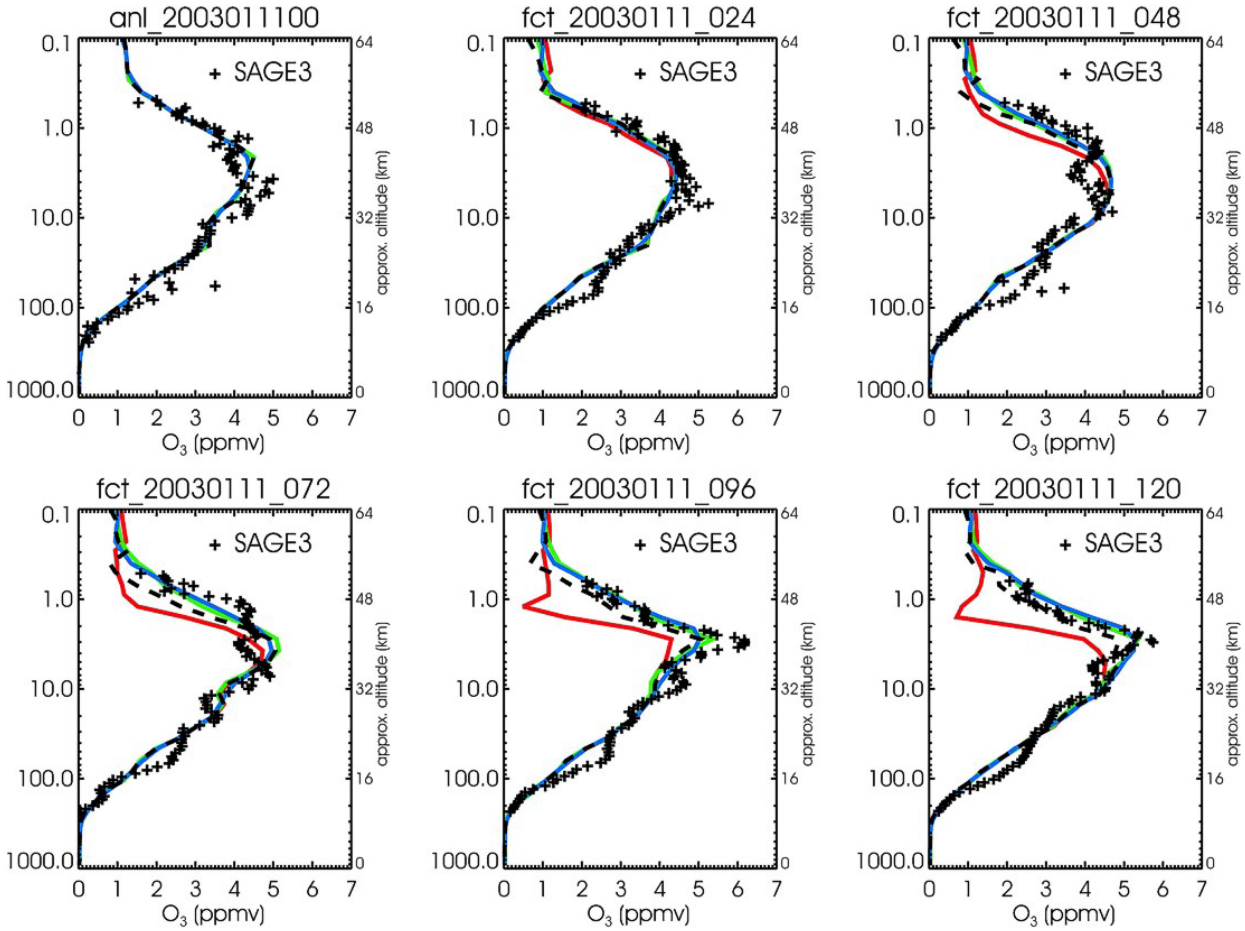

Figure 9: NOGAPS-ALPHA ozone mixing ratio forecasts (in ppmv) over Kiruna, Sweden for runs initialized on 11 January, 2003 at 0:00Z and progressing, left to right and down, in +24 hour forecast increments from analysis to +120 hour (5-day) forecasts. Black dashed curves shows passive O_3, and colored curves show active ozone using linearized photochemistry schemes from CHEM2D (green), Cariolle-Déqué (blue), and LINOZ (red). Crosses show actual ozone measurements on these days from the SAGE III satellite.

photochemistry coefficients updated using the latest version of that 2D radiation-chemistry-dynamics model (Dethof 2003). We have obtained those latest photochemical lookup tables and implemented them into a third NOGAPS-ALPHA ozone photochemistry scheme using algorithms similar to those we developed for the LINOZ scheme.

Figures 8e and 8f show the photochemical relaxation times for June and December, respectively. They show the same basic variations as the CHEM2D and LINOZ coefficients. The photochemical time scales in the lower stratosphere, while still quite long, are somewhat shorter than those in the LINOZ and CHEM2D schemes.

Intercomparison Runs

We have conducted a number of intercomparison runs, both single-column tests and full NOGAPS-ALPHA forecast runs, to assess the relative merits and performance of these three linearized ozone photochemistry schemes. Some of this work will be reported more fully elsewhere (McCormack et al. 2004), so we show only an example or two here.

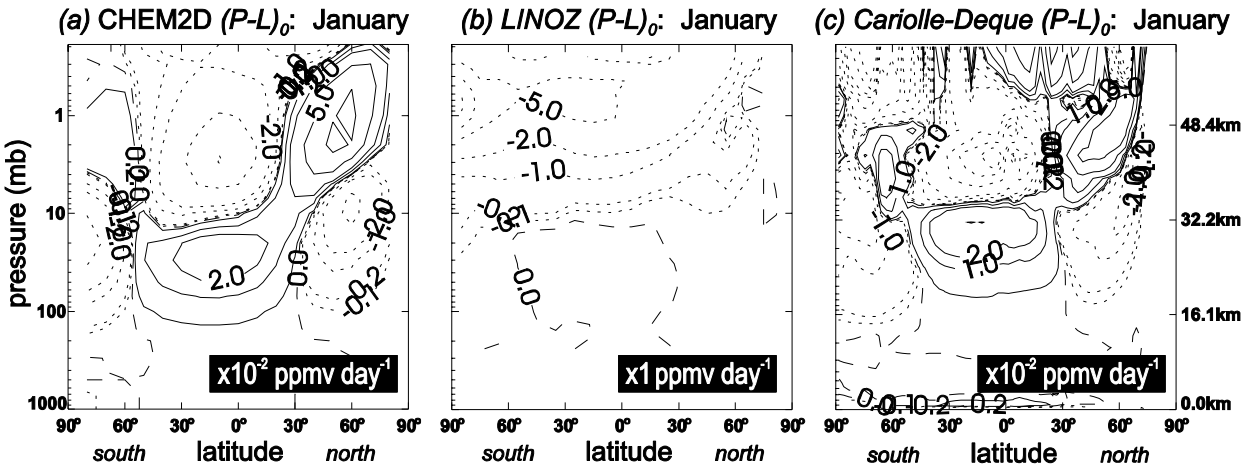

Figure 10: *(P-L)$_0$* coefficients during January for NOGAPS-ALPHA linearized O_3 photochemistry schemes based on: (a) CHEM2D coefficients; (b) LINOZ coefficients; (c) Cariolle-Déqué coefficients. CHEM2D and Cariolle-Déque contours are in units of 10^{-2} ppmv day^{-1}, while LINOZ values are in ppmv day^{-1}.

Figure 9 shows a series of NOGAPS-ALPHA 3D ozone profiles over Kiruna, Sweden from a sequence of T79L54 forecast runs initialized on 11 February 2003 (0:00Z) using MVOI/STRATOI meteorological initial conditions and 3D O_3 initialization fields from the GMAO. At this time, the second NASA SAGE III Ozone Loss and Validation Experiment (SOLVE II) was underway, with NASA's instrumented DC-8 research aircraft flying out of Kiruna (the DC-8 flew missions that measured ozone and related parameters on January 12, 14 and 16). A wealth of other data were acquired during SOLVE II, and many global models were run for this period, and so this SOLVE II period focused on Arctic winter represents an excellent focus for NOGAPS-ALPHA runs aimed at validating our emerging 3D prognostic ozone capability. On the other hand, many of these high-latitude regions during SOLVE II are in the polar night and so, unless this air was transported to lower sunlit latitudes, they may not undergo much photochemistry, making relative evaluation of the three ozone photochemistry schemes a little more difficult.

Nonetheless, Figure 9 reveals some interesting differences among predicted ozone profiles governed by each of the three-different linearized photochemistry schemes (colored curves) and passively-advected ozone (dashed curve). The most obvious feature is a systematic substantial underprediction of ozone mixing ratios on the topside of the ozone layer using the LINOZ scheme. This is a recurrent feature of nearly all of our experiments with LINOZ, both in 3D runs using NOGAPS-ALPHA and in simpler offline single-column tests. McLinden et al. (2000) comment on this propensity, attributing it to the well known "ozone deficit" problem encountered in upper stratospheric ozone modeling: however, model ozone deficits are generally smaller than this, and newer data and models now seem to have largely eliminated this discrepancy between observations and models (Siskind et al. 1998; Groos et al. 1999).

Instead, these underestimates seem to result primarily from excessively large negative equilibrium production/loss coefficients, *(P-L)$_0$*, in the LINOZ scheme in the upper stratosphere. Figure 10 compares *(P-L)$_0$* values among the three schemes for January. The CHEM2D and Cariolle-Déqué values are comparable in magnitude and have similar latitude-height distributions. Furthermore, the NCEP Global Forecasting

System (GFS) uses $(P\text{-}L)_0$ values from the Goddard two-dimensional model (Fleming et al. 2002) as their current ozone photochemistry scheme, and those values too look very similar to those in Figures 10a and 10c. The LINOZ values, on the other hand, look very different, with loss at all latitudes in the upper stratosphere and absolute values ~1-2 orders of magnitude larger than the other two schemes. We speculate that this may possibly have resulted in part from use of ozone rather than scaled odd-oxygen rates in the calculations here.

Whatever the reasons, these discrepancies make the current LINOZ scheme unsatisfactory as an ozone photochemistry parameterization for NOGAPS-ALPHA. For example, since SW O_3 heating peaks at ~1 hPa (Figure 2), underpredictions of O_3 mixing ratios of the magnitude noted for LINOZ in Figure 9 would lead to massively underestimated stratospheric heating were we to use 3D LINOZ O_3 fields in our radiation calculations.

Figure 9 also plots measured ozone profiles over this location for each forecast day from the SAGE III satellite instrument (Poole et al. 2003). While LINOZ clearly underpredicts these data, the other two schemes (CHEM2D, Cariolle-Déqué) appear to reproduce the SAGE III observations fairly well, and in this case it is difficult to distinguish any differences in skill between the two. Indeed, even passive ozone is a reasonable fit to these data, which is not surprising given the long photochemical time scales to be expected in polar night (Figure 8). There is some suggestion that ozone in the lower stratosphere (50-100 hPa) may be underpredicted: given the long photochemical time scales at all latitudes at 50-100 hPa (see Figure 8), this difference may reflect a slight error in our ozone initialization fields for this period. McCormack et al. (2004) provide a thorough study of NOGAPS-ALPHA ozone forecasts for various periods during SOLVE II.

Another useful NWP test is to compute synoptic maps of forecast total ozone, which is important, for example, in forecasting surface UV levels (Long 2003). Figure 11 shows sample NOGAPS-ALPHA total ozone forecasts initialized on 20 September 2002 during the unprecedented splitting of the Antarctic Ozone Hole due to a major stratospheric warming event (see, e.g., Allen et al. 2003, 2004). We see that NOGAPS-ALPHA captures the vortex splitting event and the separation of the Ozone Hole into two separate pieces, with the general morphology and dynamic range of the total ozone values quite similar to measurements from the Total Ozone Mapping Spectrometer (TOMS).

5. OUTLOOK

As some of the features of NOGAPS-ALPHA that we have introduced in this paper evolve and mature, they will be progressively transitioned to operations at FNMOC. The new high-altitude prognostic capabilities they will provide to NOGAPS should reap benefits in overall NWP skill and provide new forecast products of direct relevance to the Navy and the Department of Defense (DoD) generally. We conclude by discussing some of these potential benefits and new uses.

Efforts are already underway to assimilate satellite radiances directly using NAVDAS. The high-altitude capabilities of NOGAPS-ALPHA can yield considerable improvements in these assimilations. Prognostic 3D ozone, for example, can help correct complex biases in some LW radiance channels due to ozone absorption (Derber and Wu 1998). Improved operational assimilation should then lead to improvements in NWP skill at all altitudes.

There is an emerging realization that important regional winter weather influences, such as the North Atlantic Oscillation (NAO), are (in part) manifestations of a global

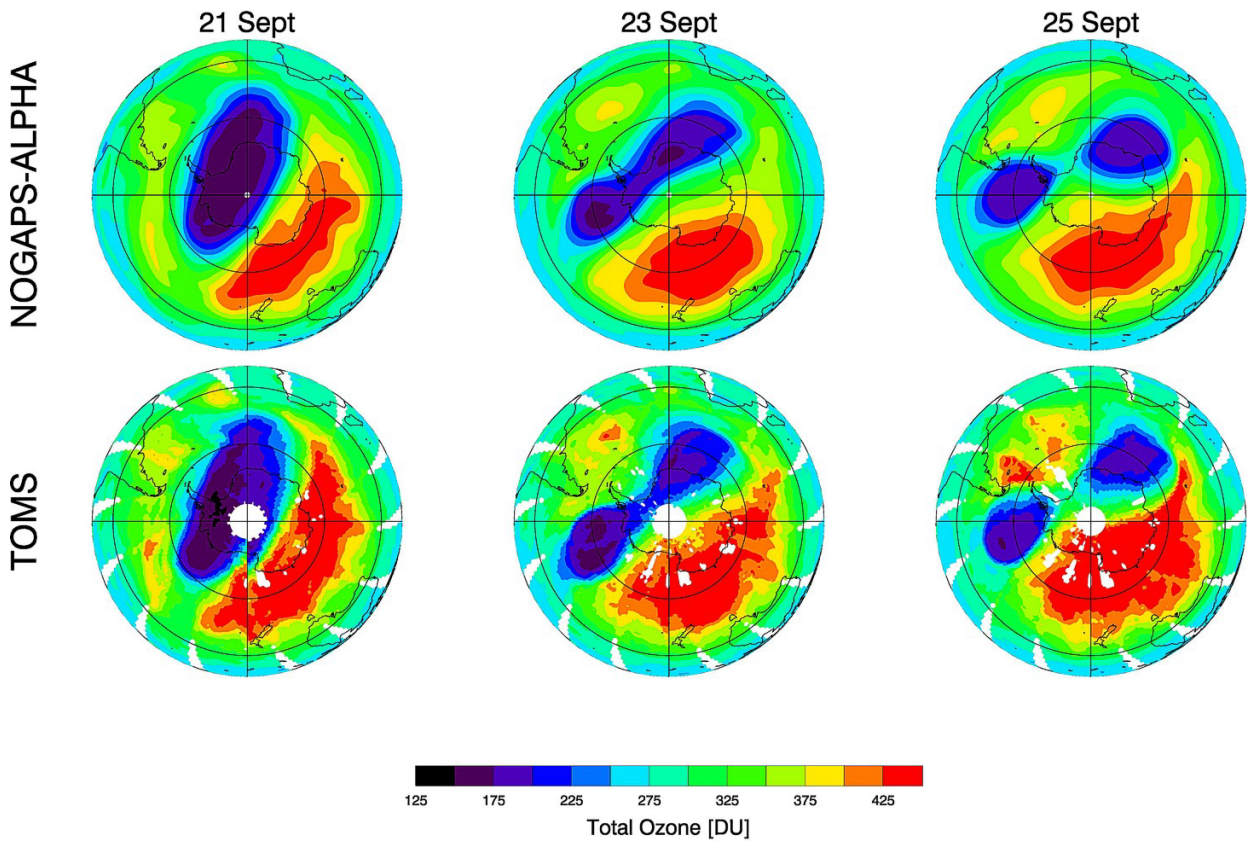

Figure 11: Top row: total ozone (in Dobson units) over the South Pole derived from NOGAPS-ALPHA T79L54 forecasts initialized on 20 September 2003 (12:00 Z) using 3D ozone initialized from GMAO analyses and updated using the Cariolle-Déqué photochemistry scheme. Results are plotted at forecast day 1 (21 September), day 3 (23 September) and day 5 (25 September). Beneath each plot is the corresponding total ozone measured on this day by TOMS.

atmospheric phenomenon known assortedly as the Arctic Oscillation (AO) or the Northern/Southern Annular Mode (NAM/SAM). Recent research has shown that anomalies in the strength of the AO often form in the upper stratosphere and then propagate downwards over a series of days, sometimes to the surface to change the state of the surface AO, NAO and hence global weather patterns (Baldwin and Dunkerton 2001; Thompson and Wallace 2002; Baldwin et al. 2003; Charlton et al. 2003). Only a high-altitude global NWP model like NOGAPS-ALPHA is capable of capturing these kinds of global AO/NAO dynamics and their effect on NWP.

Entirely new high-altitude products will be provided by a NOGAPS-ALPHA prototype running operationally, and these should serve many areas of the military, which currently lack adequate forecast guidance at stratospheric and mesospheric altitudes. Global stratospheric forecasts from NOGAPS-ALPHA would support the rapidly expanding fleet of high-altitude long-endurance (HALE) UAVs, such as Global Hawk, which are expensive airframes that cruise in the middle atmosphere, are structurally/aerodynamically vulnerable to atmospheric loads (Eckermann et al. 2004), and have almost global range. High-altitude forecasts are also needed to assess (in real-time) loads for boost-phase missile defense (Kleppner et al. 2004) and refractivity/ scintillation forecasts for the Airborne Laser (ABL) (Hecht 2004). Similar issues are relevant for DoD spacecraft launch and reentry projections, and real-time signal correction

between DoD satellites and forces/targets on the ground or in the air (e.g., UAVs). High-yield nuclear detonations inject significant volumes of radioactive debris well into the stratosphere, where it can be rapidly dispersed and transported globally (see, e.g., Figure 6). The prognostic chemical capabilities developed here for NOGAPS-ALPHA can in principle be extended to any injected tracer, and thus could be applied at short notice to provide inline global forecasts of projected dispersal and fallout of such hazardous material (e.g., Feely et al. 1966a 1966b; Rehfeld and Heimann 1995). This internal chemical transport functionality in NOGAPS-ALPHA is particularly attractive for this task, since recent work has shown that transport using the internal model dynamics of a GSM is superior compared that from offline transport models using output from assimilation systems (e.g., Schoeberl et al. 2003).

6. ACKNOWLEDGEMENTS

This work was supported in part by the Office of Naval Research though NRL's 6.2 research program. We thank Hubert Teyssedre from METEO, France, for providing the updated Cariolle-Déqué coefficients, Chris McLinden for making his LINOZ coefficients publicly available for download, Chip Trepte and the SAGE III Science Team for facilitating access to SAGE III ozone data, and Bryan Lawrence for helping us implement a version of his coupled Hines GWD scheme. Conversations on ozone photochemistry with D. E. Siskind are gratefully acknowledged.

7. REFERENCES

Alexander, M. J., and T. J. Dunkerton, 1999: A spectral parameterization of mean-flow forcing due to breaking gravity waves, *J. Atmos. Sci.,* **56**, 4167-4182.

Alexander, M. J., and K. H. Rosenlof, 2003: Gravity-wave forcing in the stratosphere: Observational constraints from the Upper Atmosphere Research Satellite and implications for parameterization in global models, *J. Geophys. Res*., **108**(D19), 4597, doi:10.1029/2003JD003373.

Allen, D. R., R. M. Bevilacqua, G. E. Nedoluha, C. E. Randall, and G. L. Manney, 2003: Unusual stratospheric transport and mixing during the 2002 Antarctic winter, *Geophys. Res. Lett*., **30 (12)**, 1599, doi:10.1029/2003GL017117.

Allen, D. R., S. D. Eckermann, L. Coy, J. P. McCormack, T. F. Hogan, and Y.-J. Kim, 2004: Stratospheric forecasting with NOGAPS-ALPHA, Paper P2.4, *Preprint Vol. Symposium on the 50th. Anniversary of Operational Numerical Weather Prediction*, American Meteorological Society, 14-17 June (this issue).

Alpert, J. C., S.-Y. Hong, and Y.-J. Kim, 1996: Sensitivity of cyclogenesis to lower tropospheric enhancement of gravity wave drag using the environmental modeling center medium range model, *Preprint Vol. 11th. Conference on Numerical Weather Prediction*, 19-23 August 1996, Norfolk, Virginia. Amer. Meteor. Soc., p. 322-323.

Arakawa, A., and V. R. Lamb, 1977: Computational design of the basic dynamical processes of the UCLA general circulation model, in *Methods in Computational Physics*, Vol. 17, J. Chang ed., Academic, 337pp.

Baker, N.L., 1992: Quality control for the Navy operational atmospheric database, *Wea. Forecasting,* **7**, 250-261.

Baldwin, M. P., and Y. J. Dunkerton, 2001: Stratospheric harbingers of anomalous weather regimes, *Science*, **294**, 581-584.

Baldwin, M. P., D. B. Stephenson, D. W. J. Thompson, T. J. Dunkerton, A. J. Charlton, and A. O'Neill, 2003: Stratospheric memory and extended-range weather forecasts, *Science*, **301**, 636-640.

Boville, B. A., 1986: Wave mean-flow interactions in a general circulation model of the troposphere and stratosphere, *J. Atmos. Sci*., **43**, 1711-1725.

Brasseur, G., and S. Solomon, 1984: *Aeronomy of the Middle Atmosphere*, Reidel Publ. Co., 441 pp.

Butchart, N., and J. Austin, 1998: Middle atmosphere climatologies from the troposphere-stratosphere configuration of the UKMO's unified model*, J. Atmos. Sci.,* **55**, 2782-2809.

Cariolle, D., and M. Déqué, 1986: Southern hemisphere medium-scale waves and total ozone disturbances in a spectral general circulation model, *J. Geophys. Res*., **91**, 10,825-10,846.

Charlton, A. J., A. O'Neill, D. B. Stephenson, W. A. Lahoz, and M. P. Baldwin, 2003: Can knowledge of the state of the stratosphere be used to improve statistical forecasts of the troposphere?, *Q. J. R. Meteorol. Soc*., **129**, 3205-3224.

Charron, M., E. Manzini, and C. D. Warner, 2002: Intercomparison of gravity wave parameterizations: Hines Doppler-spread and Warner and McIntyre ultra-simple schemes, *J. Meteorol. Soc. Japan*, **80**, 335-345.

Chou, M.-D., M. J. Suarez, X. Z. Liang, and M.-H. Yan, 2001: A thermal infrared radiation parameterization for atmospheric studies, NASA Tech. Mem. 104606, Vol. 19, Technical Reprt Series on Global Modeling and Data Assimilation, M. J. Suarez ed., 65pp.

Chou, M.-D., and M. J. Suarez, 2002: A solar radiation parameterization for atmospheric studies, NASA Tech. Mem. 10460, Vol. 15, Technical Report Series on Global Modeling and Data Assimilation, M. J. Suarez ed., 52pp.

Chun, H.-Y., and J. J. Baik, 2002: An updated parameterization of convectively forced gravity wave drag for use in large-scale models, *J. Atmos. Sci.,* **59**, 1006-1017.

Collins, W. D., J. J. Hack, B. A. Boville, P. J. Rasch, D. L. Williamson, J. T. Kiehl, B. Briegleb, J. R. McCaa, C. Bitz, S.-J. Lin, R. B. Rood, M. Zhang, and Y. Dai, 2003: Description of the NCAR community atmosphere model (CAM2), Technical Report, National Center for Atmospheric Research, Boulder, Colorado, 171 pp.

Daley, R., and E. Barker, 2001: NAVDAS: formulation and diagnostics, *Mon. Wea. Rev.,* **129**, 869-883.

Derber, J. C., and W.-S. Wu, 1998: The use of TOVS cloud-cleared radiances in the NCEP SSI analysis system, *Mon. Wea. Rev*., **126**, 2287-2299.

Dethof, A., 2003: Aspects of modelling and assimilation for the stratosphere at ECMWF, *SPARC Newsletter*, No. 21, p 11-14[1].

de Zafra, R. L., and G. Muscari, 2004: CO as an important high-altitude tracer of dynamics in the polar stratosphere and mesosphere, *J. Geophys. Res*., **109**, D06105, doi:10.1029/2003JD004099.

Douglass, A. R., R. B. Rood, and R. S. Stolarski, 1985: Interpretation of ozone temperature correlations, 2, analysis of SBUV data, *J. Geophys, Res*., **90**, 10,693-10,708.

Eckermann, S. D., J. Ma, and D. Broutman, 2004: The NRL Mountain Wave Forecast Model (MWFM), Paper P2.9, *Preprint Vol. Symposium on the 50th. Anniversary of Operational Numerical Weather Prediction*, American Meteorological Society, 14-17 June (this issue).

Emanuel, K. A., and M. Zivkovic-Rothman, 1999: Development and evaluation of a convection scheme for use in climate models, *J. Atmos. Sci.,* **56**, 1766-1782.

Errico, R. M., E. H. Barker, and R. Gelaro, 1988: A determination of balanced normal modes for two models, *Mon. Wea. Rev.,* **116**, 2717-2724.

[1] http://www.aero.jussieu.fr/~sparc/News21/21_Dethof.html

Feely, H. W., C. Barrientos, and D. Katzman, 1966a: Radioactive debris injected into the stratosphere by the Chinese nuclear weapon test of May 9, 1966, *Nature*, **212**, 1303-1304.

Feely, H. W., H. Seitz, R. J. Lagomarsino, and P. E. Biscaye, 1966b: Transport and fallout of stratospheric radioactive debris, *Tellus*, **18**, 316-328.

Fels, S. B., J. D. Mahlman, M. D. Schwarzkopf, and R. W. Sinclair, 1980: Stratospheric sensitivity to perturbations in ozone and carbon dioxide: radiative and dynamical response, *J. Atmos. Sci*., **37**, 2265-2297.

Fleming, E. L., S. Chandra, J. J. Barnett, and M. Corney, 1990: Zonal mean temperature, pressure, zonal wind, and geopotential height as functions of latitude, COSPAR International Reference Atmosphere: 1986, Part II: Middle Atmosphere Models, *Adv. Space Res.,* **10(12)**, 11-59.

Fleming, E. L., C. H. Jackman, J. E. Rosenfield, and D. B. Considine, 2002: Two-dimensional model simulations of the QBO in ozone and tracers in the tropical stratosphere, *J. Geophys. Res*., **107(D23)**, 4665, doi:10.1029/2001JD001146.

Fortuin, J.P.F., and H. Kelder, 1998: An ozone climatology based on ozonesonde and satellite measurements, *J. Geophys. Res.,* **103**, 31,709-31,734.

Fritts, D. C., and M. J. Alexander, 2003: Gravity wave dynamics and effects in the middle atmosphere, *Rev. Geophys.,* **41(1)**, 1003, doi:10.1029/2001RG000106.

Goerss, J., and R. Jeffries, 1994: Assimilation of synthetic tropical cyclone observations into the Navy Operational Global Atmospheric Prediction System, *Wea. Forecasting,* **9**, 557-576.

Goerss, J., and P. Phoebus, 1992: The Navy's operational atmospheric analysis, *Wea. Forecasting,* **7**, 232-249.

Groos, J.-U., R. Muller, G. Becker, D. S. McKenna, and P.J. Crutzen, 1999: The upper stratospheric ozone budget: An update of calculations based on HALOE data*, J. Atmos. Chem*., **34**, 171-183.

Harshvardhan, R. Davies, D. Randall, and T. Corsetti, 1987: A fast radiation parameterization for atmospheric circulation models, *J. Geophys. Res.,* **92**, 1009-1016.

Hecht, J., 2004: The airborne laser shoots for ballistic missile defense, *Laser Focus World*, **40**, 105-108.

Hines, C. O., 1997: Doppler-spread parameterization of gravity wave momentum deposition in the middle atmosphere. 2, Broad and quasi-monochromatic spectra and implementation, *J. Atmos. Sol.-Terr. Phys*., **59**, 387–400.

Hogan, T., and T. Rosmond, 1991: The description of the Navy Operational Global Atmospheric Prediction System's spectral forecast model, *Mon. Wea. Rev.* **119**, 1186-1815.

Hogan, T. F., T. E. Rosmond, and R. Gelaro, 1991: The NOGAPS forecast model: a technical description, Naval Oceanographic and Atmospheric Research Laboratory Report No. 13, 219pp.

Hogan, T. F., R. L. Pauley, and J. Teixeira, 2003: The impact of mean orography and a new gravity wave drag parameterization in NOGAPS, NRL Technical Memorandum Report, NRL/MR/7530-03-76.

Huttunen, J. T., S. Juutinen, J. Alm, T. Larmola, T. Hammar, J. Silvola, and P. J. Martikainen, 2003: Nitrous oxide flux to the atmosphere from the littoral zone of a boreal lake, *J. Geophys. Res*., **108(D14)**, 4421, doi:10.1029/2002JD002989.

Kasahara, A., 1974: Various vertical coordinate systems used for numerical weather prediction, *Mon. Wea. Rev.,* **102**,

509-522, (corrigendum, *Mon. Wea. Rev.,* **103**, 664, 1975).

Kim, Y. -J., and A. Arakawa, 1995: Improvement of orographic gravity-wave parameterization using a mesoscale gravity-wave model. *J. Atmos. Sci*., **52**, 1875-1902.

Kim, Y.-J., and J. D. Doyle, 2004: Offline evaluation of an orographic gravity-wave drag parameterization scheme extended to include the effects of orographic anisotropy and flow blocking, *Q. J. R. Meteorol. Soc*. (submitted).

Kim, Y.-J., and T. Hogan, 2004: Response of a global atmospheric forecast model to various drag parameterizations, *Tellus*, (in press).

Kim, Y.-J., S. D. Eckermann, and H.-Y. Chun, 2003: An overview of the past, present and future of gravity-wave drag parameterization for numerical climate and weather prediction models, *Atmos. Ocean,* **41**, 65-98.

Kleppner, D., F. K. Lamb, and D. E. Mosher, 2004: Boost-phase defense against intercontinental ballistic missiles, *Physics Today*, **57**, 30-35.

Limpasuvan, V., C. B. Leovy, Y. J. Orsolini, and B. A. Boville, 2000: A numerical simulation of the two-day wave near the stratopause, *J. Atmos. Sci*., **57**, 1702-1717.

Long, C. S., 2003: UV index forecasting practices around the world, *SPARC Newsletter*, No. 21, p 20-23[2].

Louis, J. F., 1979: A parametric model of vertical eddy fluxes in the atmosphere, *Boundary Layer Meteorol.,***17**, 187-202.

Louis, J. F., M. Tiedtke, and J, F, Geleyn, 1982: A short history of the operational PBL parameterization at ECMWF, *ECMWF Workshop on Planetary Boundary Parameterizations*, November 1981, 59-79.

McCormack, J. P., and D. E. Siskind, 2002: Simulations of the quasi-biennial oscillation and its effect on stratospheric H_2O, CH_4, and age of air with an interactive two-dimensional model, *J. Geophys. Res.,* **107** (D22), 4625, doi:10.1029/2002JD002141.

McCormack, J. P., S. D. Eckermann, D. R. Allen, L. Coy, T. Hogan, Y.-J. Kim, B. N. Lawrence, and A. Stephens, 2004: NOGAPS-ALPHA model simulations of stratospheric ozone and dynamics during the SOLVE2 campaign, *Atmos. Chem. Phys*., (paper in preparation).

McLinden, C. A., S. C. Olsen, B. Hannegan, O. Wild, M. J. Prather, and J, Sundet, 2000: Stratospheric ozone in 3-D models: a simple chemistry and the cross-tropopause flux, *J. Geophys. Res*., **105**, 14,653-14,665.

McPeters, R. D., D. F. Heath, and P. K. Bhartia, 1984: Average ozone profiles for 1979 from the NIMBUS 7 SBUV instrument, *J. Geophys. Res*., **89**, 5199-5214.

Neu, J. L., L. C. Sparling, and R. A. Plumb, 2003: Variability of the subtropical ‘‘edges’’ in the stratosphere, *J. Geophys. Res.*, **108**, 4482, doi:10.1029/2002JD002706.

Palmer, T. N., G. J. Shutts, and R. Swinbank, 1986: Allevation of a systematic westerly bias in general circulation and numerical weather prediction models through an orographic gravity wave drag parameterization, *Q. J. R. Meteorol. Soc*., **112**, 1001-1039.

Pawson, S., U. Langematz, G. Radek, U. Schlese, and P. Strauch, 1998: The Berlin troposphere-stratosphere-mesosphere GCM: Sensitivity to physical parameterizations, *Q. J. R. Meteorol. Soc.,* **124**, 1343-1371.

Peng, M. S., J. A. Ridout, and T. F. Hogan, 2004: Recent modifications of the Emanuel convective scheme in the Navy Operational Global Atmospheric

[2] http://www.aero.jussieu.fr/~sparc/News21/21_Long.html

Prediction System, *Mon Wea. Rev*., **132**, 1254–1268.

Poole, L. R., C. R. Trepte, V. L. Harvey, G. C. Toon, and R. L. VanValkenburg, 2003: SAGE III observations of Arctic polar stratospheric clouds – December 2002, *Geophys. Res. Lett*., **30(23)**, 2216, doi:10.1029/2003GL018496.

Rasch, P. J., and D. L. Williamson, 1990: Computational aspects of moisture transport in global models of the atmosphere, *Q. J. R. Meteorol. Soc*., **116**, 1071-1090.

Randel, W. J., 1993: Global normal-mode Rossby waves observed in stratospheric ozone data, *J. Atmos. Sci*., **50**, 406-420.

Randel, W. J., and J. C. Gille, 1991: Kelvin wave variability in the upper stratosphere observed in SBUV ozone data, *J. Atmos. Sci*., **48**, 2336-2349.

Randel, W. J., B. A. Boville, J. C. Gille, P. L. Bailey, S. T. Massie, J. B. Kumer, J. L. Mergenthaler, and A. E. Roche, 1994: Simulation of stratospheric N_2O in the NCAR CCM2: comparison with CLAES data and global budget analysis, *J. Atmos. Sci*., **51**, 2834-2845.

Randel, W. J., F. Wu, A. Gettelman, J. M. Russell III, J. M. Zawodny, and S. J. Oltmans, 2001: Seasonal variation of water vapor in the lower stratosphere observed in Halogen Occultation Experiment data, *J. Geophys. Res*., **106**, 14,313-14,325.

Randel, W., P. Udelhofen, E. Fleming, M. Geller, M. Gelman, K. Hamilton, D. Karoly, D. Ortland, S. Pawson, R. Swinbank, F. Wu, M. Baldwin, M.-L. Chanin, P. Keckhut, K. Labitzke, E. Remsberg, A. Simmons, and D. Wu, 2004: The SPARC intercomparison of middle-atmosphere climatologies, *J. Climate*, **17**, 986-1003.

Rehfeld, S., and M. Heimann, 1995: Three dimensional atmospheric transport simulation of the radioactive tracers ^{210}Pb, ^{7}Be, ^{10}Be, and ^{90}Sr, *J. Geophys. Res*., **100**, 26,141-26,161.

Sangster, W. E., 1960: A method of representing the horizontal pressure force without reduction of station pressures to sea level, *J. Meteor*., **17**, 166-176.

Scanlon, T. M., and G. Kiely, 2003: Ecosystem-scale measurements of nitrous oxide fluxes for an intensely grazed, fertilized grassland, *Geophys. Res. Lett*., **30(16)**, 1852, doi:10.1029/2003GL017454.

Schoeberl, M. R., A. R. Douglass, Z. Zhu, and S. Pawson, 2003: A comparison of the lower stratospheric age spectra derived from a general circulation model and two data assimilation systems, *J. Geophys. Res*., **108(D3)**, 4113, doi:10.1029/2002JD002652.

Shepherd, T. G., K. Semeniuk, and J. N. Koshyk, 1996: Sponge layer feedbacks in middle-atmosphere models, *J. Geophys. Res.,* 101, 23447-23464.

Simmons, A. J., and D. M. Burridge, 1981: An energy and angular momentum conserving vertical finite-difference scheme and hybrid vertical coordinates, *Mon. Wea. Rev.,* **109**, 758-766.

Simmons, A. J., and R. Strüfing, 1983: Numerical forecasts of stratospheric warming events using a model with a hybrid vertical coordinate, *Q. J. R. Meteorol. Soc.*, **109**, 81-111.

Simmons, A. J., B. J. Hoskins, and D. M. Burridge, 1978: Stability of semi-implicit time scheme, *Mon. Wea. Rev.,* **106**, 405-412.

Siskind, D. E., L. Froidevaux, J. M. Russell, and J. Lean, 1998: Implications of upper stratospheric trace constituent changes observed by HALOE for O_3 and ClO from 1992 to 1995, *Geophys. Res. Lett*., **25**, 3513-3516.

Slingo, J. M., 1987. The development and verification of a cloud prediction scheme

in the ECMWF model, *Q. J. R. Meteorol. Soc*., **113**, 899-927.

Smith, A. K., P. Preusse, and J. Oberheide, 2002, Middle atmosphere Kelvin waves observed in Cryogenic Infrared Spectrometers and Telescopes for the Atmosphere (CRISTA) 1 and 2 temperature and trace species, *J. Geophys. Res.*, **107(D23)**, 8177, doi:10.1029/2001JD000577.

Stajner, I., L. P. Riishojgaard, and R. B. Rood, 2001: The GEOS ozone data assimilation system: Specification of error statistics, *Q. J. Roy. Meteorol. Soc.*, **127**, 1069-1094.

Stolarski, R. S., and A. R. Douglass, 1985: Parameterization of the photochemistry of stratospheric ozone including catalytic loss processes, *J. Geophys. Res*., **90**, 10,709-10,718.

Summers, M. E., D. E. Siskind, J. T. Bacmeister, R. R. Conway, S. E. Zasadil, and D. F. Strobel, 1997: Seasonal variation of middle atmospheric CH_4 and H_2O with a new chemical-dynamical model, *J. Geophys. Res.*, **102**, 3503-3526.

Swinbank R., and D. A. Ortland, 2003: Compilation of wind data for the Upper Atmosphere Research Satellite (UARS) Reference Atmosphere Project, *J. Geophys. Res.*, **108** (D19), 4615, doi:10.1029/2002JD003135.

Teixeira, J. and T. Hogan, 2002: Boundary layer clouds in a global atmospheric model: Simple cloud cover parameterization, *J. Climate,* **15**, 1261-1276.

Thompson, D. W. J., and J. M. Wallace, 2002: Stratospheric connection to Northern Hemisphere wintertime weather: Implications for prediction, *J. Climate*, **15**, 1421-1428.

Tiedtke, M., 1984: The sensitivity of the time-scale flow to cumulus convection in the ECMWF model, *Workshop on Large-Scale Numerical Models, 28 Nov- 1 Dec 1983, ECMWF*, 297-316.

Trenberth, K. E., and D. P. Stepaniak, 2002: A pathological problem with NCEP reanalyses in the stratosphere, *J. Climate*, **15**, 690-695.

Urban, J., et al., 2004, The northern hemisphere stratospheric vortex during the 2002–03 winter: Subsidence, chlorine activation and ozone loss observed by the Odin Sub-Millimetre Radiometer, *Geophys. Res. Lett*., **31**, L07103, doi:10.1029/2003GL019089.

Webster, S., A. R. Brown, D. R. Cameron, and C. P. Jones, 2003: Improvements to the representation of orography in the Met Office Unified Model, *Q. J. R. Meteorol. Soc.*, **129**, 1989-2010.